Proceedings of the ASME 2019
2nd International Offshore Wind Technical Conference
IOWTC2019
November 3-6, 2019, St. Julian's, Malta

IOWTC2019-7620

EXPERIMENTAL VALIDATION OF ANGULAR VELOCITY MEASUREMENTS FOR WIND TURBINES DRIVETRAIN CONDITION MONITORING

Farid K. Moghadam
Department of Marine Technology
Norwegian University of Science and Technology
7491 Trondheim, Norway
Email: farid.k.moghadam@ntnu.no

Amir R. Nejad
Department of Marine Technology
Norwegian University of Science and Technology
7491 Trondheim, Norway
Email: amir.nejad@ntnu.no

ABSTRACT

Drivetrain bearings are seen as the most common reason of the wind turbine drivetrain system failures and the consequent downtimes. In this study, the angular velocity error function is used for the condition monitoring of the bearings and gears in the wind turbine drivetrain. This approach benefits from using the sensor data and the dedicated communication network which already exist in the turbine for performance monitoring purposes. Minor required modification includes an additional moderate sampling frequency encoder without any need of adding an extra condition monitoring system. The additional encoder is placed on the low speed shaft and can also be used as the backup for the high speed shaft encoder which is critical for turbine control purposes. A theory based on the variations of the energy of response around the defect frequency is suggested to detect abnormalities in the drivetrain operation. The proposed angular velocity based method is compared with the classical vibration-based detection approach based on axial/radial acceleration data, for the faults initiated by different types of excitation sources. The method is experimentally evaluated using the data obtained from the encoders and vibration sensors of an operational wind turbine.

INTRODUCTION

Application of condition-based fault detection for early stage fault detection and the consequent reduction of the system downtime is a motivation for using a condition monitoring system for the wind turbine drivetrain which consists of large/massive/expensive components with a high failure rate [1]. Vibration analysis is one of the most common approaches used for condition monitoring of different subsystems of the wind turbine *e.g.* structure, blades, platform and drivetrain [2]. Vibration analysis is a category of signal-based condition monitoring approaches which comprises different time and frequency domain analyses. Axial and radial acceleration vibration measurements are widely used for condition monitoring of the wind turbine drivetrain components [3]. Axial and radial vibrations in the drivetrain as a rotational system are resulted by axial and lateral forces caused by synergistic effects of external excitation forces, internal excitations and unbalanced/misalignment in the system. Therefore, by the analysis of acceleration, velocity and displacement by using acceleration vibration and displacement sensors data, it is possible to predict faults by the evaluation of the defect consequences in the system response. In the recent literature of vibration analysis for condition monitoring of the drivetrain *e.g.* by Nejad et al. [4] and Sankar et al. [5], the application of angular velocity measurements for condition monitoring of gearbox is suggested. In [5], the power spectral density (PSD) of an angular velocity measurement is directly used for the fault detection in a gearbox. In [4], the energy of the residual of angular velocity measurements obtained from the different positions of a $5MW$ high fidelity wind turbine drivetrain model is used for the gearbox fault detection. The inherent robustness of the residual signal to noise and external disturbances, and the sensitivity to fault is the motivation for using this approach [6]. Ghane et al. [7] has reported the successful application of an angular velocity residual-based detection approach for detection of a fault in one of the bearings of the intermediate planetary stage gear of the

gearbox. Drivetrain as a rotating system is encountered with torsional vibrations. Therefore, monitoring of angular velocity provides useful information about torsional excitations which seems to be really helpful for condition monitoring of this system. For this purpose, the angular velocity time series obtained from the speed encoders, and the resultant angular displacement and angular acceleration obtained by applying conditioning circuits on the angular velocity measurements can be used. The theoretical justification is the direct relation between the torque as the load and the angular displacement as the response.

Time domain vibration analysis is an attempt to extract useful information for fault detection from vibration measurements by monitoring the variation of peak, mean, standard deviation and root-mean-square (r.m.s) of the acceleration, velocity and displacement of the measurements over the time [8–10]. However, the frequency domain analysis takes advantage of fast Fourier transform (FFT) and PSD of the signal which helps to find the defect frequencies and defective components [11]. The conventional vibration-based condition monitoring of the wind turbine dirvetrain system is based on a time domain analysis for the detection supported by a frequency domain analysis for the localization of the fault [12]. The time domain analysis is based on the r.m.s value of the axial/radial acceleration and velocity vibration in mm/s and m/s^2, and the peak value of displacement in μm obtained from the accelerometers time series data, where these values should not exceed the predefined limits suggested by the standards ISO 10816-21 and ISO 13373-1 respecting to the rotational frequency and type of application. The idea behind the complementary frequency domain analysis is that each defect in any specific component happens with a particular frequency which helps to find the source of the fault and the defective component.

This paper is an experimental validation of the angular velocity error function approach originally proposed by Nejad et al. [4]. The slightly modified angular velocity residual function demonstrates a higher performance in extracting information required for the detection of abnormal cases. To reach the angular velocity residual, in addition to the high-speed shaft encoder which is typically embedded in the wind turbine drivetrain for performance monitoring and control purposes, an additional encoder is installed on the low-speed side. Starting with presenting a classification on different types of internal/external and torsional/non-torsional excitations which influence on the wind turbine drivetrain operation, the performance of angular velocity measurements and angular velocity residual signal for detection of abnormalities are studied and compared with the conventional condition monitoring method based on axial/radial acceleration data for each category of excitation. The study is mainly in the frequency domain, and the analysis tools are FFT, PSD, envelope PSD and energy spectral density. The amplitude demodulation method with the use of envelope spectrum is a complementary tool which is used in the literature (*e.g.* by [7]) to improve the PSD performance in the detection of defects in bearings and gears. On this basis, the contributions of this paper are:

1. Classification of different excitations and available vibration-based detection solutions,
2. Experimental comparison between different available solutions for bearings and gears defects initiated by different types of excitations,
3. Experimental validation of angular velocity residual approach which is recently proposed in the literature of vibration-based condition monitoring of wind turbine drivetrain,
4. Experimental comparison between different frequency domain tools for detecting abnormalities in the system.

The remainder of the paper is organized as follows. In *Methodology*, different vibration-based condition monitoring approaches and the applied frequency domain analysis tools are discussed. Experimental simulations to validate the discussed drivetrain condition monitoring approaches are presented in *Experimental results and simulations* followed by conclusions.

METHODOLOGY

Test system

The under consideration test system is the drivetrain of a less than $2MW$ operational wind turbine. The data includes the acceleration and angular velocity sensors installed in different points of the drivetrain obtained by the sampling frequency $25600Hz$. The accelerometers are placed on the housing and the encoders are located on the shaft. The drivetrain topology and the placement of sensors are shown in Fig. 1. The details of the sensors and the drivetrain specification are provided in Tables 1 and 2, respectively. The encoder EN1 is added to the system to experimentally evaluate the angular velocity error function approach.

In the following, two different methods, the first based on the axial/radial acceleration data obtained from accelerometers, and the second based on the angular velocity measurements by using the speed encoders data are elaborated.

Axial/radial acceleration-based condition monitoring

The vertical displacement X as the response of a one degree of freedom system with the mass m, stiffness k, damping c under the sinusoidal excitation force F in the non-dimensional form can be expressed by

$$X = \frac{\frac{F_0}{k}}{\sqrt{(1-(\frac{\omega}{\omega_n})^2)^2 + (2\zeta(\frac{\omega}{\omega_n}))^2}}, \quad (1)$$

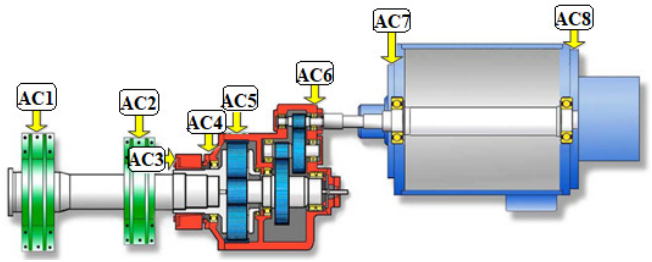

(a) *Acceleration sensors placement*

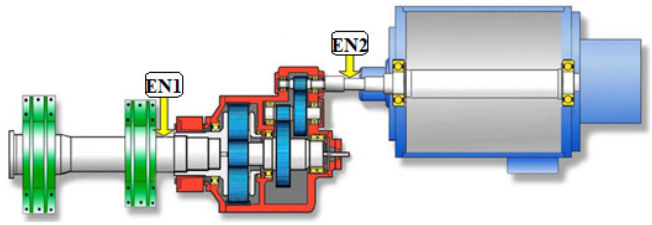

(b) *Angular velocity sensors placement*

FIGURE 1: Drivetrain topology, accelerometers and encoders placement.

TABLE 1: Sensors specification.

Sensor	Description
AC1	Front main bearing accelerometer (radial)
AC2	Rear main bearing accelerometer (radial)
AC3	Gearbox input shaft accelerometer (axial)
AC4	Gearbox input shaft bearing accelerometer (radial)
AC5	Gearbox medium-speed bearing accelerometer (radial)
AC6	Gearbox high-speed shaft bearing accelerometer (radial)
AC7	Front generator bearing (radial)
AC8	Rear generator bearing (radial)
EN1	Low-speed shaft encoder (radial)
EN2	High-speed shaft encoder (radial)

where F_0 and ω are the amplitude and frequency of the excitation force, respectively. ω_n and ζ are the natural frequency and the damping ratio of the system defined by

$$\omega_n = \sqrt{\frac{k}{m}}, \quad \zeta = \frac{c}{c_c} \quad and \quad c_c = 2m\omega_n.$$

Therefore, a large amplitude in the frequency spectrum of response X at frequency ω can be due to either an amplified internal/external excitation, or due to a resonance resulted by the coincidence of the excitation frequency ω with one of the natural

TABLE 2: Under consideration drivetrain specification.

Rated rotor speed (rpm)	19,68
Rated generator speed (rpm)	1544
Gearbox topology	$planetary - parallel - parallel$
Gear ratio	$1:5.1667 \times 1:3.8889 \times 1:3.9048$

frequencies of the system. The latter can be used as an indicator of the abnormalities in the system operation. Without the loss of generality, the idea can be extended to a system with a higher number of masses and a higher degree of freedom. The latter motivates the application of frequency domain tools to monitor the frequency content of response and consequently determine the sources of the abnormalities. For this purpose, FFT and PSD of axial/radial acceleration data can provide useful information. The normalized CooleyTukey FFT algorithm is used to observe the capability of acceleration measurements in distinguishing abnormalities, which is defined by $X(j\omega) = \int_{-\infty}^{+\infty} x(t)e^{-i\omega t}dt$, where $X(j\omega)$ is the the spectrum of the response x.

Afterwards, the PSD and subsequently the energy of the signal around the suspicious frequency is used as the abnormality detection tool in the paper. The PSD of x is defined by

$$S_{xx}(\omega) = \frac{|X(j\omega)|^2}{n}, \tag{2}$$

where S_{xx} is the PSD spectrum of x. The energy of the frequency domain signal X in the frequency range $[\omega 1\ \omega 2]$ is then calculated by

$$E = \frac{1}{\pi}\int_{\omega 1}^{\omega 2} |X(j\omega)^2|\, d\omega. \tag{3}$$

The PSD of the envelope of the signal x obtained by using Hilbert transform is used as the other abnormality detection tool. The Hilbert envelope of x and the PSD of the envelope signal are defined by

$$\widetilde{X}(j\omega) = X(j\omega)(-j.sgn(\omega)), \quad S_{\widetilde{x}\widetilde{x}}(j\omega) = \frac{|\widetilde{X}(\omega)|^2}{n}, \tag{4}$$

where $\widetilde{X}$ and $S_{\widetilde{x}\widetilde{x}}$ are the envelope and envelope PSD spectrums of x, and sgn is the signum function. Subsequently, the energy of $\widetilde{X}$ is used for the fault detection purpose.

It is worth noting that the vibration response is basically the summation (and not the multiplication) of a wide range of sinusoidal signals with different frequencies and amplitudes. The envelope or the amplitude demodulation of such a signal shows in its FFT all the frequencies of the signal plus a number of sidebands which are the combinations of the different frequency components of the signal. Feng et al. [13] has proposed a model for the vibration response of a planetary gearbox, where the amplitude demodulated signal of the vibration response contains all the combinations of the system and defect frequencies. The latter does not characterize any filtering feature of the envelope analysis to distinguish the defect frequencies from the system resonance frequencies.

The spectral envelope is also the envelope curve of the amplitude spectrum and a smoothed version of the signal spectrum which wraps tightly around the magnitude spectrum, linking the peaks of the spectrum [14]. The latter is widely used for sound processing applications, and shows some features in highlighting the peaks of the PSD spectrum of the signal. The resultant can provide a smoother and more noise resilient signal which can be used as the input signal in the third energy-based detection tool in the paper. The spectral envelope of $S_{xx}(\omega)$ by using the Hilbert transform is defined by

$$\widetilde{S}_{xx}(\omega) = \frac{1}{\pi}\int_{-\infty}^{\infty}\frac{S_{xx}(\Omega)}{\omega-\Omega}d\Omega. \tag{5}$$

In the paper, since the measurements are discretized in time, the normalized energy based on the normalized length-n discrete Fourier transform is used, where n is the spectrum frequency resolution. The normalization in this context means a division by $\sqrt{n}$ for FFT which is equivalent to a division by n for the PSD of the signal. Two different energy indices EI^1 and EI^2 are then calculated as

$$EI^1 = \frac{E^*}{E},\ EI^2 = \frac{E^*_{\omega_s}}{E_{\omega_s}}. \tag{6}$$

where * is used as the indicator for the suspicious data set. E and E^* are the energy over all the frequency horizon of normal and suspicious cases, respectively. ω_s is the frequency horizon which covers the suspicious frequency $\omega_s{}^*$ and 10% below and above it. E_{ω_s} is the energy of the acceleration signal in the frequency range ω_s filtered by the band-pass filter $H(\omega_s)$, $X(\omega_s) = X(\omega)H(\omega_s)$, and $E^*_{\omega_s}$ is the same parameter of the suspicious case. The performance of these two indices is demonstrated in the numerical results section.

The other incentive for using the signal energy-based analyses is the direct relation between the energy and the r.m.s value of the signal, $x_{r.m.s} = 0.5\sqrt{E}$, which avails to find thresholds for energy-based methods by taking advantage of the available standards.

Angular velocity-based condition monitoring

As mentioned earlier, rotational motion of the drivetrain system and the torsional behavior of most the drivetrain loads motivate the application of angular velocity for the condition monitoring of the drivetrain components. The latter can provide insight regarding the excitation sources and drivetrain system properties as inputs for condition monitoring of the system.

The equation (1) which describes the response in a system with a linear motion can be extended to the system with a rotational motion as

$$\theta = \frac{\frac{\tau_0}{k_t}}{\sqrt{(1-(\frac{\omega}{\omega_n})^2)^2 + (2\zeta_t(\frac{\omega}{\omega_n}))^2}}, \tag{7}$$

where θ is the angular position and τ_0 is the amplitude of the excitation momentum. For this case, ω_n is the natural torsional frequency of the system. k_t is the torsional stiffness of the shaft, and ζ_t is the torsional damping ratio.

Therefore, by the evaluation of the torsional response, it could be possible to find the amplified torsional excitation frequencies. Even though there is not any torque measurement device in the system, but the angular velocity analysis is expected to provide similar information about the torsional vibrations due to the relation between torque and angular velocity. The angular velocity signals obtained by the two speed encoders embedded on the high-speed and low-speed shafts are studied. Similar to the procedure explained in the previous part, the frequency spectrum, PSD and energy of the two sets angular velocity time series data are studied and the possibility to observe and detect amplified excitations and abnormalities is studied. The possibility of using angular velocity-based energy indices to extract useful information for detection of different types of abnormalities is discussed in the numerical results section. The continued part describes the method based on the angular velocity measurements *i.e.* by using the angular velocities residual signal.

Angular velocity error function The angular velocity residual/error function e_{total} observed in the high-speed side of the drivetrain is expressed by [15]

$$e_{total} = N_{HS} - \alpha_1\alpha_2\alpha_3 N_{LS}, \tag{8}$$

where N_{HS} and N_{LS} are the rotational speed in rpm obtained from the high- and low-speed encoders, respectively. α_1, α_2 and α_3 are the inverse of gear ratios of the gearbox stages. Gear ratio

as per definition is $\frac{N_{in}}{N_{out}}$, where N_{in} and N_{out} are the speeds of input and output shafts, respectively. The FFT, PSD and energy of the angular velocity residual signal e_{total} and the individual angular velocity measurements for the detection of different types of abnormalities are studied in the next section.

EXPERIMENTAL RESULTS AND DISCUSSIONS

The drivetrain components can be excited by different sources of internal/external and torsional/non-torsional excitations. In the Table 3, the different excitation sources, their types and impacts on the under consideration land-based wind turbine drivetrain are listed. With respect to the different types of excitation sources, different test cases are designed in the following. In *scenario one*, the system responses including axial/radial accelerations, angular velocity measurements and angular velocities residual signal are studied under internal and non-torsional drivetrain excitations. In *scenario two*, the drivetrain responses under internal and torsional excitations are evaluated. In *scenario three*, the responses are studied under external and torsional drivetrain excitation sources.

Scenario one: internal and non-torsional excitations

In the test scenario one, it is assumed that the abnormality source causes axial/radial motions in the system. The under consideration internal excitation source is the helical gear mesh frequency of the third stage of gearbox which is resulted due to the defective gear teeth and causes axial/radial vibrations in the system. The latter can be observed at the mesh frequency of the high-speed stage gear, $f_m = 529Hz$, in the frequency spectrum of the radial and axial acceleration sensors installed in different locations of the gearbox and the main bearings. However, the abnormality is not observable by the generator acceleration sensors.

Fig. 2 shows the frequency spectrum of the gearbox accelerometers, speed encoders and angular velocity error around the excitation frequency. The high-amplitude excitation at $f = 529Hz$ in this figure can represent either an excited natural frequency by the excitation frequency or an amplified internal excitation due to an abnormality in the excitation source. As it can be seen in Fig. 2, the under consideration abnormality is observable by the acceleration measurements but non-observable by angular velocity signals. The normalized energy indices EI^1 and EI^2 of all the acceleration and angular velocity signals under a rated operation of the suspicious drivetrain are presented in Table 4. Our extensive observations showed that for different sets of operational data, the threshold 3 can provide a criterion to evaluate if the abnormality can be detected by the energy method applied on the associated sensor. Based on this explanation, the energy index EI^1 is not performing well in detection of the abnormalities, and the energy index EI^2 is preferred based on the simulation study. The higher values of this index can represent both the severity of the abnormality and the higher capability of the sensor in observing it. The better visibility of the aforedescribed gear problem in $AC5$ signal is due to the transfer of the resultant load of the gear mesh excitation from the high speed stage gear to lower stage gears through the tooth contact between the stages. The direct contact between the ring gear of the first stage of gearbox and the housing transfers the mentioned load directly to $AC5$ sensor which results in a better visibility of the abnormality by $AC5$. The latter, transpires that the acceleration measurements on the planetary stages could be of a higher importance for the detection of problems in the gears. The mentioned abnormality does not reveal any sign in the angular velocity measurements and the angular velocity residual signal, because it does not produce any significant vibration in the rotational direction. Since the source of excitation is non-torsional, the frequency of occurrence is expected to be the same for the different measurement points. Therefore, the abnormality is seen with the same frequency in the acceleration data of the different sensors located in different places of the drivetrain.

As it can be seen in Table 5, the described abnormality cannot be detected by the conventional time domain approach based on the evaluation of the r.m.s value of the acceleration time series data.

Scenario two: internal and torsional excitations

The performance of the angular velocity signals and the selected acceleration measurements in distinguishing an internal torsional excitation induced by generator electromagnetic torque oscillations is demonstrated in Fig. 3 (P is the frequency of the voltage main component).

The induction generator electromagnetic torque oscillations happen significantly with the voltage frequency $50Hz$ and the third order harmonics as a consequence of the current and back emf harmonics caused by power electronic converter and the grid low power quality, and the second harmonic as a result of voltage unbalanced operations, [16,17]. The cogging effects between the stator and rotor teeth also result in the torque oscillation whose frequency depends on the numbers of machine slots and may not happen in integer multiples of $50Hz$. As it can be seen in Fig. 3, these abnormalities are observable by angular velocity error function but non-observable by acceleration measurements. There is a high possibility that these excitation frequencies coincide the defect frequencies of the generator and gearbox high-speed stage bearings which are among the most important reasons of failure in the geared drivetrains equipped with high-speed generators. The performance of angular velocity energy indices for detecting the mentioned abnormality in the system is shown in Table 6.

TABLE 3: Drivetrain excitation sources.

Excitation	Frequency range	Type (internal/external)	Vibration (torsional/non-torsional)
Gears defect (Hz)	$0-550$	*Internal*	$Non-torsional$
Bearings defect (Hz)	$0-220$	*Internal*	$Non-torsional$
Turbine rotational motion (Hz)	$0-0.32$	*External*	*Torsional*
Tower shadow (Hz)	$0-0.97$	*External*	$Torsional/non-torsional$
Wind (Hz)	$0-0.02$	*External*	$Torsional/non-torsional$
Electromagnetic torque oscillations (Hz)	$0-3000$	*Internal*	*Torsional*

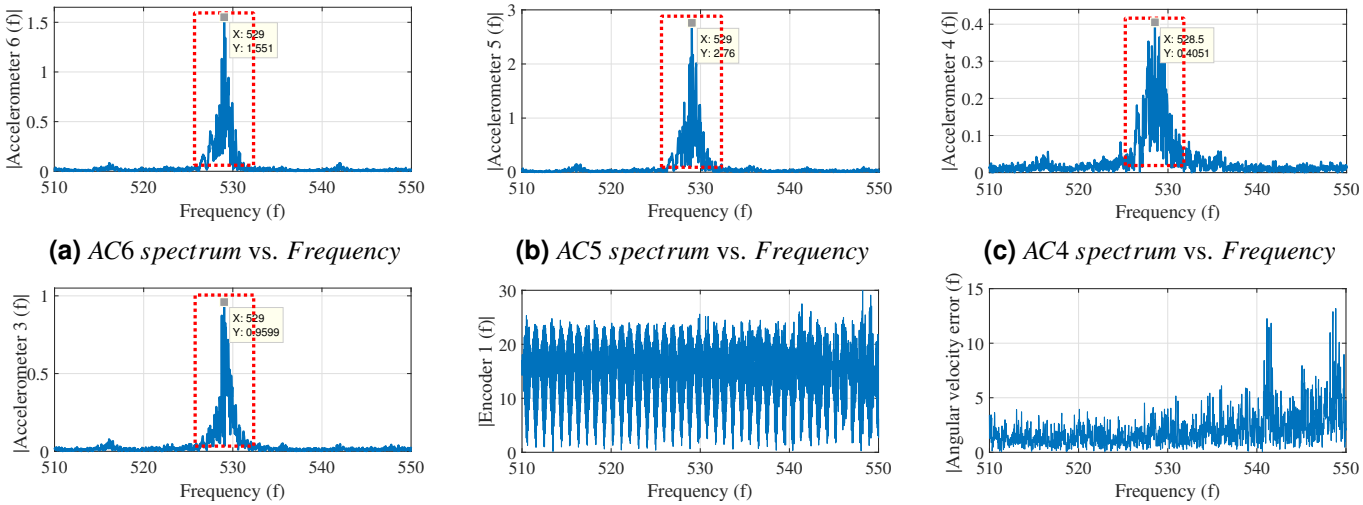

(a) *AC*6 *spectrum* vs. *Frequency* **(b)** *AC*5 *spectrum* vs. *Frequency* **(c)** *AC*4 *spectrum* vs. *Frequency*

(d) *AC*3 *spectrum* vs. *Frequency* **(e)** *EN*1 *spectrum* vs. *Frequency* **(f)** e_{total} vs. *Frequency*

FIGURE 2: First test scenario.

TABLE 4: Calculated energy indices for the suspicious frequency $\omega^* = 529Hz$.

Criterion \ Sensor	*AC*1	*AC*2	*AC*3	*AC*4	*AC*5	*AC*6	*AC*7	*AC*8	*EN*1	*EN*2	e_{total}
EI^1	1.64	2.41	2.19	2.25	1.66	1.38	0.92	0.96	1.01	1.01	1.06
EI^2	4.71	17.17	25.14	3.19	25.30	7.00	1.11	1.00	1.01	1.00	0.87

Scenario three: external and torsional excitations

Fig. 4 shows the low frequency content of the under consideration signals. As it can be seen, in the angular velocity signals of EN1 and EN2, two amplified frequencies are observed. Regrading the very low frequency content of them, it is expected that these frequencies are excited by drivetrain external excitation sources. The first occurs at $0.05Hz$ which could be the first tower side-side natural frequency of a soft-soft design excited by wind due to the wind impulsive behavior [18]. The performance of energy index approach in distinguishing this abnormality is

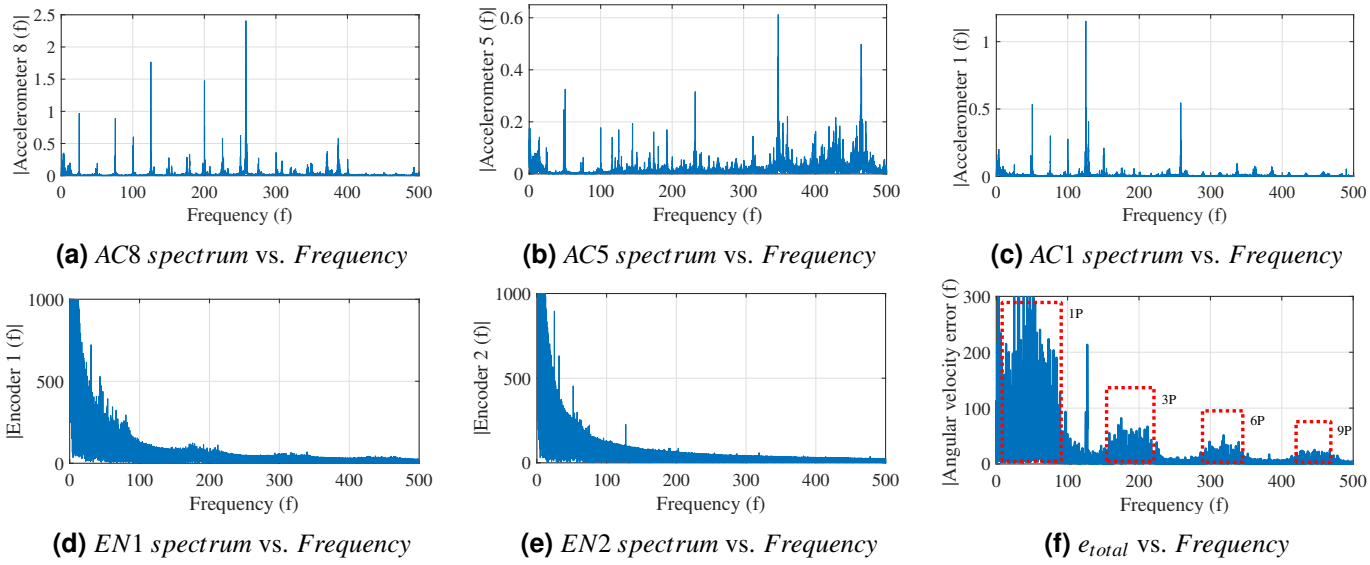

(a) *AC*8 *spectrum* vs. *Frequency* **(b)** *AC*5 *spectrum* vs. *Frequency* **(c)** *AC*1 *spectrum* vs. *Frequency*

(d) *EN*1 *spectrum* vs. *Frequency* **(e)** *EN*2 *spectrum* vs. *Frequency* **(f)** e_{total} vs. *Frequency*

FIGURE 3: Second test scenario.

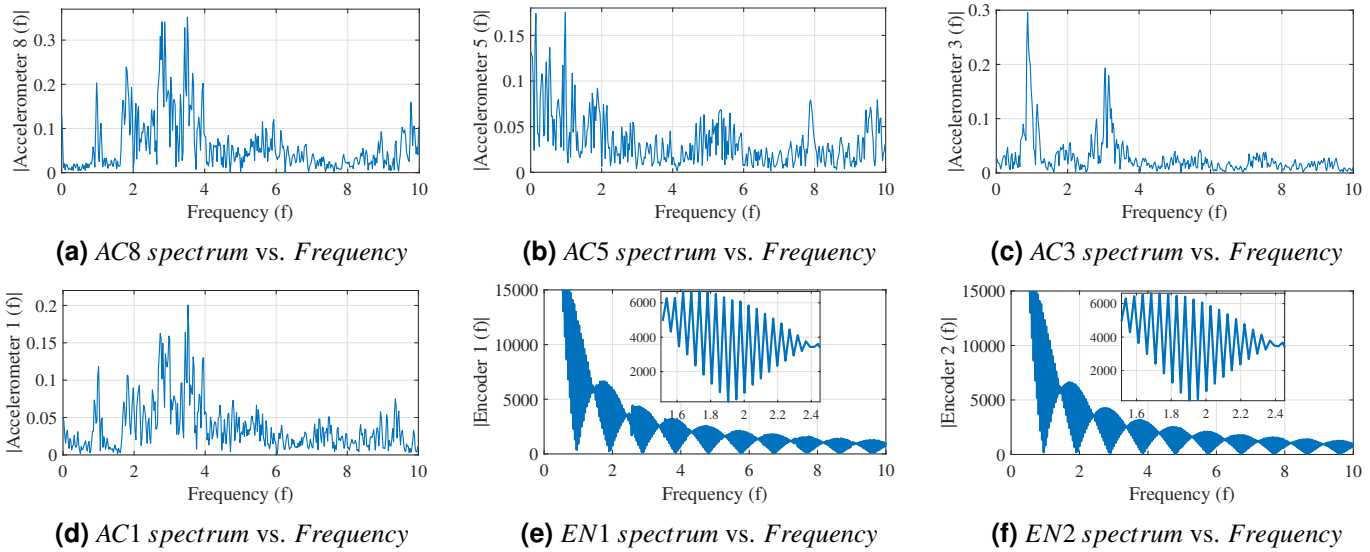

(a) *AC*8 *spectrum* vs. *Frequency* **(b)** *AC*5 *spectrum* vs. *Frequency* **(c)** *AC*3 *spectrum* vs. *Frequency*

(d) *AC*1 *spectrum* vs. *Frequency* **(e)** *EN*1 *spectrum* vs. *Frequency* **(f)** *EN*2 *spectrum* vs. *Frequency*

FIGURE 4: Third Test scenario.

shown in Table 7.

The other happens with the harmonics of $0.97Hz$ which coincides the blade passing frequency as a consequence of tower shadow excitation effect. As it can be seen in Fig. 4, these excitations are observable by angular velocity measurements but not observable by acceleration data. The external excitations are filtered from angular velocity residual so that these excitations are not observable by the angular velocity error function.

The excited frequencies in the torsional response does not necessarily represent a defect in the system, but provides valuable insights about the torsional loads which can influence on the drivetrain components but may not be considered in the design step. An amplified frequency in angular velocity spectrum can represent either an abnormal internal/external torsional excitation source which can considerably affect the fatigue life of the system, or an amplified torsional frequency. These impacts are not necessarily observed on the spectrum of acceleration data due to either the pollution of the frequency domain signal around those frequencies or the non-force impacts of those excitation.

The performance of PSD of the *AC*5 acceleration signal and

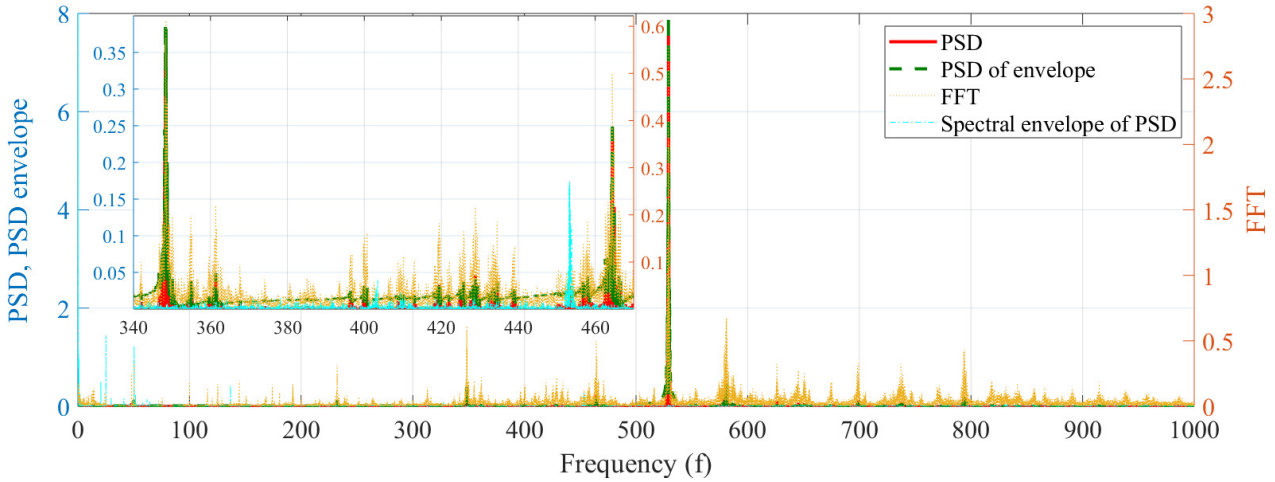

FIGURE 5: PSD, PSD of envelope, FFT and spectral envelope of PSD of AC5 acceleration signal.

TABLE 5: Acceleration r.m.s compared with the warning limits brought in standard ISO 10816-21.

Comparison \ Sensor	$AC3$	$AC4$	$AC5$	$AC6$
Measured r.m.s (m/s^2)	0.04	0.03	0.07	0.06
Standard r.m.s threshold (m/s^2)	0.3	0.3	0.3	7.5

TABLE 6: Calculated energy indices for the suspicious frequency $\omega^* = 170Hz$.

Criterion \ Sensor	$EN1$	$EN2$	e_{total}
EI^1	1.01	1.01	1.06
EI^2	2.21	1.97	26.47

its envelope compared with the spectral envelope of PSD and the FFT of signal in extracting the useful information is demonstrated in Fig. 5. As it can be seen, PSD and spectral envelope of PSD show a higher performance in extracting features out of the signal. The slightly higher performance of spectral envelope of PSD compared to PSD by cancellation of some peaks due to random vibrations, and smoother and greater amplification of the signal at the defect frequencies is shown in the figure. The spectral envelope cancels the influences of random vibrations due to wind turbulences and drivetrain transients which can bury the harmonics associated with the components defect frequencies in the standard FFT spectrum. In PSD of envelope, additional sidebands as the combination of system and defect frequencies are added compared to PSD. The figure also clearly shows the lower performance of standard FFT due to the background noises. Based on this study, to compromise between the simplicity and accuracy, the PSD of the signal is selected as the input of energy method in the simulation studies.

TABLE 7: Calculated energy indices for the suspicious frequency $\omega^* = 0.05Hz$.

Criterion \ Sensor	$EN1$	$EN2$	e_{total}
EI^1	1.01	1.01	1.06
EI^2	7.97	7.96	0.64

CONCLUSION

The experimental evaluation of angular velocity error function showed a potential in distinguishing internal torsional excitations, whereas this category of excitations were not observable with neither acceleration sensors nor individual speed encoders. Even though the acceleration measurements perform well in detecting non-torsional internal excitations, but the impacts of torsional excitations are either lost in the polluted FFT signal or not significant so that cannot be detected in early stages by acceleration measurements. In addition, the individual angular velocity

measurements reveals the external torsional excitations, whereas both the acceleration measurements and angular velocity residual signal do not disclose them. The application of angular velocity measurements and angular velocity error function for better evaluation of the excitation sources and the subsequent earlier stage detection of abnormalities initiated by torsional excitations is suggested.

ACKNOWLEDGMENT

The authors would like to thank Kongsberg Digital AS, Trondheim, Norway, for providing experimental data for this study.

REFERENCES

[1] Tchakoua, P., Wamkeue, R., Ouhrouche, M., Slaoui-Hasnaoui, F., Tameghe, T., and Ekemb, G., 2014. "Wind turbine condition monitoring: State-of-the-art review, new trends, and future challenges". *Energies,* ***7***(4), pp. 2595–2630.

[2] Márquez, F. P. G., Tobias, A. M., Pérez, J. M. P., and Papaelias, M., 2012. "Condition monitoring of wind turbines: Techniques and methods". *Renewable Energy,* ***46***, pp. 169–178.

[3] Zhang, Z., Verma, A., and Kusiak, A., 2012. "Fault analysis and condition monitoring of the wind turbine gearbox". *IEEE transactions on energy conversion,* ***27***(2), pp. 526–535.

[4] Nejad, A. R., Odgaard, P. F., and Moan, T., 2018. "Conceptual study of a gearbox fault detection method applied on a 5-MW spar-type floating wind turbine". *Wind Energy,* ***21***(11), pp. 1064–1075.

[5] Roy, S. K., Mohanty, A., and Kumar, C., 2015. "Amplitude demodulation of instantaneous angular speed for fault detection in multistage gearbox". In *Vibration Engineering and Technology of Machinery*. Springer, pp. 951–961.

[6] Hwang, I., Kim, S., Kim, Y., and Seah, C. E., 2010. "A survey of fault detection, isolation, and reconfiguration methods". *IEEE transactions on control systems technology,* ***18***(3), pp. 636–653.

[7] Ghane, M., Nejad, A. R., Blanke, M., Gao, Z., and Moan, T., 2017. "Diagnostic monitoring of drivetrain in a 5 MW spar-type floating wind turbine using hilbert spectral analysis". *Energy Procedia,* ***137***, pp. 204–213.

[8] Mathew, J., and Alfredson, R., 1984. "The condition monitoring of rolling element bearings using vibration analysis". *Journal of vibration, acoustics, stress, and reliability in design,* ***106***(3), pp. 447–453.

[9] Večeř, P., Kreidl, M., and Šmíd, R., 2005. "Condition indicators for gearbox condition monitoring systems". *Acta Polytechnica,* ***45***(6).

[10] Stander, C., Heyns, P., and Schoombie, W., 2002. "Using vibration monitoring for local fault detection on gears operating under fluctuating load conditions". *Mechanical Systems and Signal Processing,* ***16***(6), pp. 1005–1024.

[11] Hameed, Z., Hong, Y., Cho, Y., Ahn, S., and Song, C., 2009. "Condition monitoring and fault detection of wind turbines and related algorithms: A review". *Renewable and Sustainable energy reviews,* ***13***(1), pp. 1–39.

[12] Son, J., Kang, D., Boo, D., and Ko, K., 2018. "An experimental study on the fault diagnosis of wind turbines through a condition monitoring system". *Journal of Mechanical Science and Technology,* ***32***(12), pp. 5573–5582.

[13] Feng, Z., and Zuo, M. J., 2012. "Vibration signal models for fault diagnosis of planetary gearboxes". *Journal of Sound and Vibration,* ***331***(22), pp. 4919–4939.

[14] Schwarz, D., 1998. "Spectral envelopes in sound analysis and synthesis". PhD thesis, Citeseer.

[15] Nejad, A. R., Odgaard, P. F., Gao, Z., and Moan, T., 2014. "A prognostic method for fault detection in wind turbine drivetrains". *Engineering Failure Analysis,* ***42***, pp. 324–336.

[16] Kiani, M., and Lee, W.-J., 2008. "Effects of voltage unbalance and system harmonics on the performance of doubly fed induction wind generators". In 2008 IEEE Industry Applications Society Annual Meeting, IEEE, pp. 1–7.

[17] Moghadam, F. K., Ebrahimi, S., Oraee, A., and Velni, J. M., 2018. "Vector control optimization of dfigs under unbalanced conditions". *International Transactions on Electrical Energy Systems,* ***28***(8), p. e2583.

[18] van der Tempel, J., and Molenaar, D.-P., 2002. "Wind turbine structural dynamics–a review of the principles for modern power generation, onshore and offshore". *Wind engineering,* ***26***(4), pp. 211–222.